Mechanical stress distribution and the utilisation of the magneto-elastic effect in electrical machines

Jan Karthaus, Benedikt Groschup, Robin Krüger and Kay Hameyer
Institute of Electrical Machines (IEM), RWTH Aachen University, Aachen, Germany

Received 2 October 2018
Revised 31 January 2019
Accepted 1 February 2019

Abstract

Purpose – Due to the increasing amount of high power density high-speed electrical machines, a detailed understanding of the consequences for the machine's operational behaviour and efficiency is necessary. Magnetic materials are prone to mechanical stress. Therefore, this paper aims to study the relation between the local mechanical stress distribution and magnetic properties such as magnetic flux density and iron losses.

Design/methodology/approach – In this paper, different approaches for equivalent mechanical stress criteria are analysed with focus on their applicability in electrical machines. Resulting machine characteristics such as magnetic flux density distribution or iron are compared.

Findings – The study shows a strong influence on the magnetic flux density distribution when considering the magneto-elastic effect for all analysed models. The influence on the iron loss is smaller due to a high amount of stress-independent eddy current loss component.

Originality/value – The understanding of the influence of mechanical stress on dimensions of electrical machines is important to obtain an accurate machine design. In this paper, the discussion on different equivalent stress approaches allows a new perspective for considering the magneto-elastic effect.

Keywords Electrical machines, Iron losses, Iron loss modelling, Soft magnetic materials, Mechanical stress, Magneto-elastic coupling

Paper type Research paper

1. Introduction

Increased power density of electric drives for automotive applications can be achieved by increasing the rotor speed. As a consequence, high mechanical stress occurs within the rotor lamination. The magnetic flux density and the iron loss of the soft magnetic material is influenced by this mechanical stress (magneto-elastic effect). Several publications present models to describe the mechanical stress dependency of magnetic hysteresis (Aydin *et al.*, 2017), magnetic flux density or iron loss (Leuning *et al.*, 2016). A majority of the presented models relate to magnetic measurements, where electrical steel sheet is subject to mechanical stress. Usually, uniaxial measurements are performed, which means that the applied mechanical stress is collinear to the magnetic field (Karthaus *et al.*, 2017). With these measurements, simple relations of mechanical stress-dependent magnetic properties can be determined. However, there are also approaches to perform biaxial measurements, where the direction of mechanical stress and magnetic field varies for a two-dimensional case (Aydin *et al.*, 2016). In electrical machines, the local mechanical stress distribution do not represent simple one-dimensional cases and can be very complex. Therefore, a detailed understanding of the mechanical stress distribution, which has many origins, inside the

COMPEL - The international journal for computation and mathematics in electrical and electronic engineering
Vol. 38 No. 4, 2019
pp. 1085-1097

0332-1649
DOI 10.1108/COMPEL-10-2018-0387

rotor stack lamination has to be studied. The link between a complex mechanical stress distribution and its consequences for the magnetic properties is essential for an improved electrical machine design resulting, for example, in less iron losses.

This paper focusses on the detailed study of the mechanical stress distribution in rotors of electrical machines. Different approaches for equivalent stresses are compared and their appropriate use in electrical machines is discussed. Therefore, a detailed methodology is presented. This study compares the influence of the different models on machine quantity such as magnetic flux density distribution or iron loss.

2. Modelling of the magneto-elastic effect

To model the influence of a multi-dimensional stress load in the soft magnetic material on the electromagnetic properties, a simplification to a tensor-based quantity is required. In a 3-D body, stress conditions such as shown in Figure 1 (left) can be found. On each side of the element, normal stresses σ and shear stresses τ in the three dimensions of the coordinate system x, y, and z apply. For mechanical comparison of the stress load in electric motors' rotor lamination 2-D plane stress conditions to calculate the load of the rotor are applied (Groschup and Leonardi, 2017; Balluff *et al.*, 2018). The same 2-D assumptions are used for the calculation of the magneto-elastic effect. Thereby, a simplified stress state is assumed such as shown in Figure 1 right.

The stress tensor for the two-dimensional case can be described by:

$$\boldsymbol{\sigma} = \begin{pmatrix} \sigma_{\mathrm{x}} & \tau_{\mathrm{xy}} \\ \tau_{\mathrm{yx}} & \sigma_{\mathrm{y}} \end{pmatrix} \tag{1}$$

In the later discussion, principal stresses are used. By performing a principal axis transformation with angle α, an equivalent stress state without shear stresses can be derived (Figure 1 right):

$$\boldsymbol{\sigma}' = \begin{pmatrix} \sigma_1 & 0 \\ 0 & \sigma_2 \end{pmatrix}, \tag{2}$$

where σ_1 and σ_2 are the principal stress components.

The magneto-elastic effect can be measured by using uniaxial single sheet tester attached to a hydraulic cylinder such as described in Karthaus *et al.* (2017). The results can

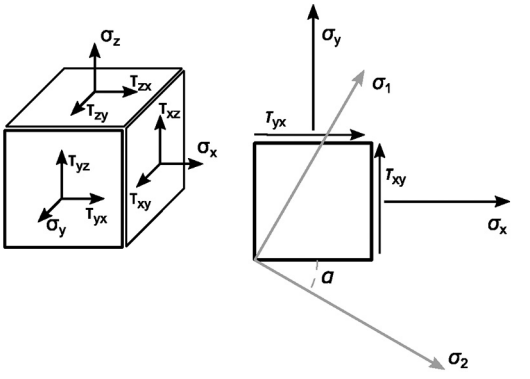

Figure 1.
Mechanical stresses in 3-D and 2-D bodies

be used to determine mechanical stress-dependent material parameters such as permeability or iron loss dependency. Due to the test setup, measurements are restricted to collinear measurement of magnetic field and mechanical stress direction. A stress criterion is necessary to compare an arbitrary stress condition in the electric machine with measured magnetic properties.

In Figure 2, the mechanical load conditions of the uniaxial and biaxial case are shown including the directions of the principal stresses σ_1 and σ_2 and magnetic flux density $\mathbf{B}$. In the uniaxial case like used in the test setup, the directions of the magnetic field density $\mathbf{B}$ and the principal stress σ match. In the biaxial case like found in real application, the principal stress in the second dimension σ_2 is not zero. Further, the direction of the magnetic field $\mathbf{B}$ is not necessarily correlated to the direction of one of the principal stress components σ_1 and σ_2. The direction of the magnetic flux density $\mathbf{B}$ and the principal stress σ_1 deviates by the magnetisation angle β_h.

2.1 Presentation of models

In the approach according to Balluff *et al.* (2018), the Von Mises (VM) stress is assigned to the determined measured values under uniaxial load. The VM stress criterion theory is also called Distortion-Energy (DE) theory because it predicts yielding when the distortion strain energy of an element reaches or exceeds the distortion strain energy for yield in simple compression or tension. The equivalent stress tensor is calculated based on the formula (Läpple, 2016):

$$\sigma_{\mathrm{VM}} = \sqrt{\sigma_{\mathrm{x}}^2 - \sigma_{\mathrm{x}}\sigma_{\mathrm{y}} + \sigma_{\mathrm{y}}^2 + 3\tau_{\mathrm{xy}}^2} \tag{3}$$

It is assumed that the VM stress σ_{VM} corresponds to the uniaxial loading $\sigma_{\mathrm{uniaxial}}$ applied in the test specimen by:

$$\sigma_{\mathrm{VM}} = \sigma_{\mathrm{uniaxial}} \tag{4}$$

To determine compressive or tensile load condition, the sign of the larger principal stress is used:

$$\sigma_{\mathrm{eq,VM}} = \begin{cases} \mathrm{sgn}(\sigma_1)\,\sigma_{\mathrm{VM}}, \text{ if } |\sigma_1| > |\sigma_2| \\ \mathrm{sgn}(\sigma_2)\,\sigma_{\mathrm{VM}}, \text{ if } |\sigma_2| > |\sigma_1| \end{cases} \tag{5}$$

This model was introduced in Balluff *et al.* (2018) and is called Model 0 in the following discussions.

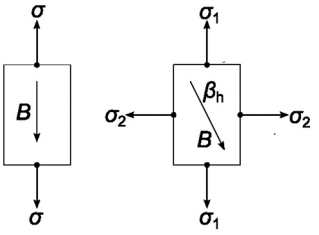

Figure 2.
Mechanical load cases

Model 1 is introduced by Daniel and Hubert (2009). The model is based on magneto-elastic energy conservation and includes the directions of principal stresses σ_1, σ_2 and the magnetic flux density $\mathbf{B}$ as it is shown in Figure 3. The equivalent stress $\sigma_{\mathrm{eq,dir}}$ is defined as:

$$\sigma_{\mathrm{eq,dir}} = \left(\sigma_1 - \frac{1}{2}\sigma_2\right)h_1^2 + \left(\sigma_2 - \frac{1}{2}\sigma_1\right)h_2^2 \tag{6}$$

With the unit vector $\mathbf{h}$ in direction of the magnetic field density $\mathbf{B}$ (Yamazaki and Fukushima, 2015). h_1 and h_2 are the components of $\mathbf{h}$ in the direction of the principal stress components σ_1 and σ_2. The vector components h_1 and h_2 are used as weighting factors for the calculation of the equivalent stress $\sigma_{\mathrm{eq,dir}}$. The angle φ_σ is used to determine the position of the principal mechanical stress relative to the global x–y coordinate system. The unit vector $\mathbf{h}$ is aligned to the magnetic flux density $\mathbf{B}$. The consideration of the directions of principal stresses and magnetic field vector is an advantage of the methodology.

Model 2 is proposed by Daniel (2013) and is based on the conservation of magneto-elastic energy by equal initial susceptibilities under different mechanical loads. The equivalent stress $\sigma_{\mathrm{eq,susc}}$ can be described by:

$$\sigma_{\mathrm{eq,susc}} = \frac{1}{\alpha}\ln\left(\frac{2\exp(\alpha\tilde{\sigma}_{\mathrm{x}})}{\exp(\alpha\tilde{\sigma}_{\mathrm{y}}) + 1}\right) \tag{7}$$

With:

$$\alpha = \frac{9\chi_0\lambda_{\mathrm{s}}}{2\mu_0 M_{\mathrm{s}}^2}. \tag{8}$$

χ_0 describes the magnetic susceptibility, λ_{s} the saturation magnetostriction and M_{s} the saturation magnetisation. In this model, $\tilde{\sigma}_{\mathrm{x}}$ and $\tilde{\sigma}_{\mathrm{y}}$ are the mechanical normal stress components. Therefore, the stress state needs to be transformed using Mohr's circle so that $\tilde{\sigma}_{\mathrm{x}}$ is collinear and $\tilde{\sigma}_{\mathrm{y}}$ is perpendicular to the direction of the magnetic field. The shear stress component in this stress state is not considered in the model (Yamazaki *et al.*, 2018). The model is based on a simplified description of the magnetic field which is subject to the energetic equilibrium magnet behaviour. According to Daniel (2013), the methodology is not comprehensively applicable for materials with highly anisotropic or heterogeneous

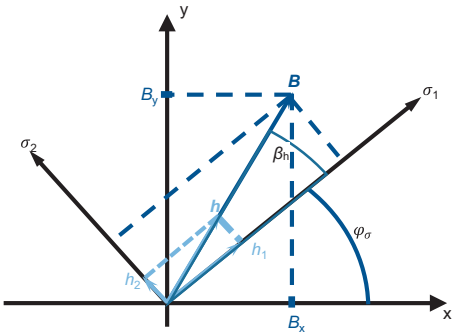

Figure 3.
Visualisation of direction-dependent equivalent stress

properties and for fast rotation of magnetisation. The method can be used for low magnetic fields under assumption of isotropic behaviour (Daniel, 2013).

The equivalent stress presented by Schneider and Richardson (Daniel and Hubert, 2009) (Model 3) can be determined by the simplified equation using the value of the principal stress components σ_1 and σ_2:

$$\sigma_{\mathrm{eq,SR}} = \sigma_1 - \sigma_2 \tag{9}$$

The directions of the magnetic flux density $\mathbf{B}$ and of the first principal stress σ_1 must match as a condition of applicability.

The equivalent stress model according to Sablik (Model 4) is based on a micro-magnetic model, which considers the direction-dependent relationship between σ_1 and magnetic field (Sablik *et al.*, 1994). For biaxial loads, the equivalent stress of the model can be calculated by:

$$\sigma_{\mathrm{eq,Sablik}} = \begin{cases} \frac{1}{3}(2\sigma_1 - \sigma_2) & \text{if } \sigma_1 < 0\,, \\ \frac{1}{3}(\sigma_1 - 2\sigma_2) & \text{if } \sigma_1 \geq 0 \end{cases} \tag{10}$$

As a function of the sign of the principal stress σ_1, which needs to be parallel to the external magnetic field. σ_2 is the value of the second principal stress tensor in plane stress condition.

2.2 Comparison of models

The previously introduced Models 3 and 4 require defined proportion of the directions of the magnetic flux density $\mathbf{B}$ and the principal stress components σ_1 and σ_2. This simplification is not predominant in real electrical rotor laminations. Therefore, Models 3 and 4 are not used in the subsequent comparison.

First, Model 2 is compared to Model 0. Figure 4 shows the equivalent stresses $\sigma_{\mathrm{eq},\pm\mathrm{VM}}$ and $\sigma_{\mathrm{eq,susc}}$ as functions of the values of the principal stress components σ_1 and σ_2. For this

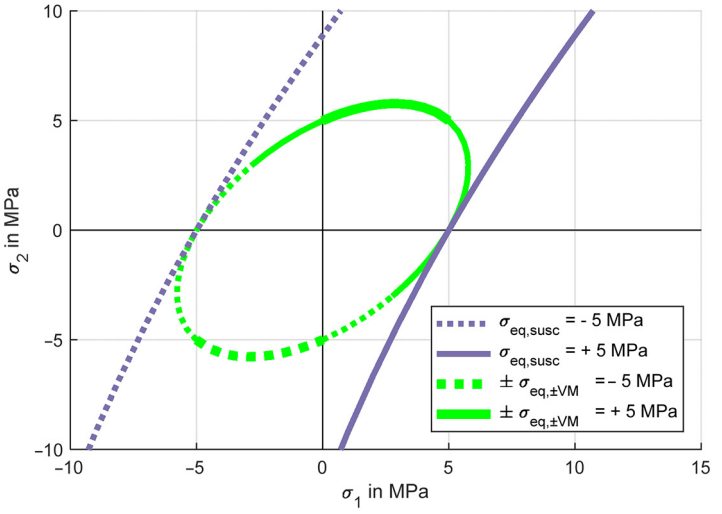

Figure 4.
Comparison of $\sigma_{\mathrm{eq},\pm\mathrm{VM}}$ and $\sigma_{\mathrm{eq,susc}}$

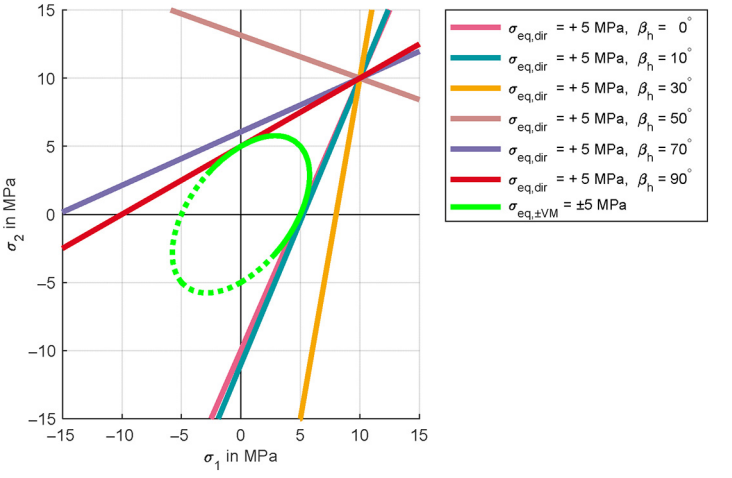

Figure 5.
Comparison of Model 0 and Model 1

comparison, it is assumed that the direction of B is collinear to the direction of σ_1. With this assumption, σ_1 is equal to $\tilde{\sigma}_x$ that is used in Model 2.

The elliptical curve represents the von Mises stress for the scalar value of $\sigma_{eq,\pm VM} = \pm 5$ MPa. This means that all points on this curve are defined by the respective combinations of the principal stresses σ_1 and σ_2 for $\sigma_{eq,\pm VM} = \pm 5$ MPa. The sign of $\sigma_{eq,\pm VM}$ is indicated by the sign of the higher principal stress and therefore, the ellipse is divided into two areas. At the transition of the two areas, the model predicts an equivalent stress value with changing sign. This rapid change of material properties is physically not reasonable. The left curve is always assigned to the negative equivalent stress value and the right curve corresponds to the positive value. Related values for $\sigma_{eq,\pm VM}$ and $\sigma_{eq,susc}$ are predicted for small values of σ_2. In all other areas, the approaches lead to significantly deviating equivalent stresses.

In Figure 5, equivalent stresses of Model 1 $\sigma_{eq,dir}$ and Model 0 $\sigma_{eq,\pm VM}$ are compared. As Model 1 considers the difference between the direction of magnetic flux density **B** and the principal stress components σ_1 and σ_2, the equivalent stress $\sigma_{eq,dir}$ is plotted for different angles β_h (6). For simplification, only the positive equivalent stress values $\sigma_{eq,dir}$ are shown. For different angles β_h, the linear curves have different gradients and intersections with the ordinate. However, all curves have one common point of intersection with the values of the principle stresses ($\sigma_1 = \sigma_2 = 10$ MPa) twice the value of the direction-adjusted equivalent stress ($\sigma_{eq,dir} = 5$ MPa).

3. Consideration in electrical machines: example interference fit

3.1 Simulation chain

In the mechanical simulation, not only production but also operating influences on mechanical stresses can be considered. The most significant mechanical load caused by machine operation in high speed application is the centrifugal load (Karthaus and Hameyer, 2017). In the mechanical simulation tool, the local deformation and the principal stresses are calculated for the rotor and extracted in dependency of the location (Figure 6). In this study, the stator is not affected by mechanical stress. For the electromagnetic simulation, the deformed rotor geometry must be combined with the stator of the machine and is meshed triangularly. Then, the electromagnetic simulation is performed. The mechanical stress distribution is transferred to the

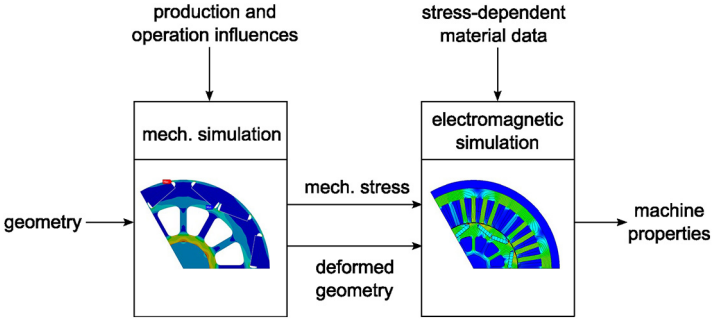

Figure 6.
Simulation chain

electromagnetic machine model. For each element, the information of the mechanical stress in the centre is provided. With the knowledge of the mechanical stress distribution inside the machine, the magneto-elastic effect can be implemented. In the simulation, the relative magnetic permeability is provided locally as a function of the mechanical uniaxial stress and the magnetic flux density via stress-dependent material data. These data are extracted from the measurement results presented in Karthaus *et al.* (2018). To calculate the equivalent mechanical stress for Models 1 and 2, the information about the magnetic flux density direction is required. Therefore, a first simulation without the mechanical stress consideration is performed. With knowledge of the magnetic flux density distribution, the machine properties, average torque and iron losses in the rotor can be determined. For this study, a permanent magnet synchronous machine is used. The operating point is chosen with a speed of n = 10,000 rpm where high centrifugal forces occur. In this study, only the effect of mechanical stress on the rotor is investigated. The centrifugal forces are superposed with the mechanical stress coming from the interference fit of shaft and rotor lamination stack.

3.2 Mechanical stress distribution: interference fit

The interference fit is simulated with an diametrical interference of 0.0245 mm. The press fit is designed to cause von Mises stress $\sigma_{\mathrm{eq},\pm\mathrm{VM}}$ slightly below yield strength of the material. The stress distribution of the three equivalent stress models inside the rotor are shown in Figure 7. Model 0 as well as Model 2 show high mechanical stresses at the shaft–hub connection. For Model 2, the mechanical stress components collinear and perpendicular to the direction of magnetic flux density are calculated. Model 0 shows negative equivalent stress values with a rapid change of sign at the transition bridges next to the inner pockets of the lamination. This transition is the result of the previously discussed rapid transition of the distinction of cases, which is physically not explicable.

In Figure 7(c), the direction-adjusted equivalent stress is shown. Significant deviations from the other equivalent stress models can be recognised. In most areas, where the magnetic vector is in the radial direction, Model 1 results in a negative value. However, there are exceptions: In some fillets, the tangential component of the mechanical stress is almost non-existent. As a result, the direction-adapted model of equivalent stresses shows no negative stress values in these areas. Near the shaft–hub connection, high negative stress values up to −173 MPa occur.

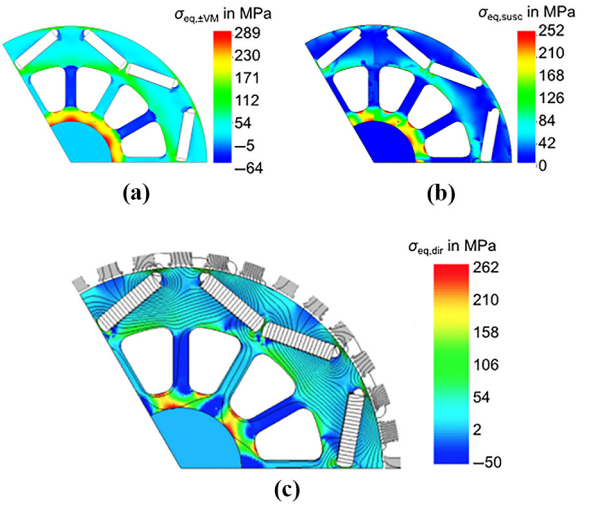

Figure 7.
Equivalent mechanical stresses for interference fit

Notes: (a) Model 0: Sign-dependent von Mises stress; (b) Model 2: Susceptibility-based equivalent stress; (c) Model 1: Direction-dependent stress

3.3 Magnetic flux density distribution

The differences in the equivalent stress models lead to different distributions of the magnetic flux densities inside the rotor. Figure 8(a) shows the magnetic flux density distribution B_0 without consideration of the magneto-elastic effect. Figure 8(b)-(d) show the difference between the magnetic flux densities without and with consideration of the magneto-elastic effect. In general, Model 0 and Model 1 lead to higher differences in magnetic flux density than Model 2 due to the existence of negative stress values for this simulated case.

For compressive stress, a significantly reduced relative magnetic permeability was measured (Karthaus *et al.*, 2018). According to this, areas with negative stress values lead to significant differences of the magnetic flux density. This effect can be seen for Model 1 between the magnet fillets and the outer edge of the rotor. Due to the high magnetic flux densities in the bridges, the magnet fillets and the outer diameter of the rotor, the high mechanical stress has no effect on the magnetic flux density. In conclusion, the magnetic flux densities is significantly altered when considering the magnetic-mechanical effect.

3.4 Iron loss

Another important quantity of the electric machine is the iron loss. In particular, the iron loss $p_{Fe,tot}$ represents an elementary loss component. The iron loss can be distinguished to hysteresis (p_{hys}), eddy current (p_{cl}), excess (p_{exc}) and non-linear losses (p_{nl}) (Eggers *et al.*, 2012). In this section, the iron losses in the rotor of the machine are analysed considering the magneto-elastic effect. The iron losses for the reference machine without magneto-elastic effects shown in Figure 9. The eddy current losses are the biggest contribution to the total iron losses. Hysteresis and excess losses in the rotor, however, are lower. The total iron

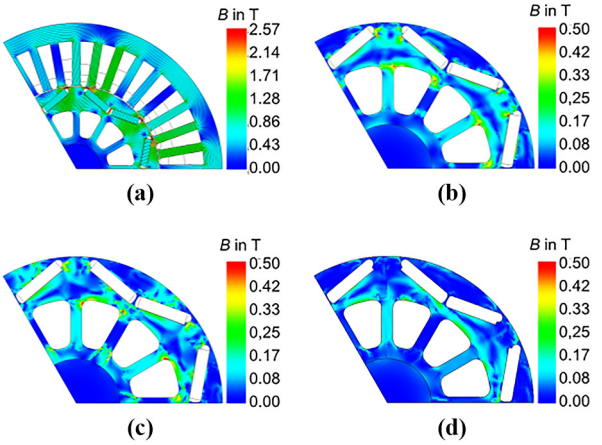

Notes: (a) B_0; (b) Model 0: $|B_0 - B_{eq,\pm VM}|$; (c) Model 1: $|B_0 - B_{eq,dir}|$; (d) Model 2: $|B_0 - B_{eq,susc}|$

Figure 8.
Magnetic flux density distributions and differences

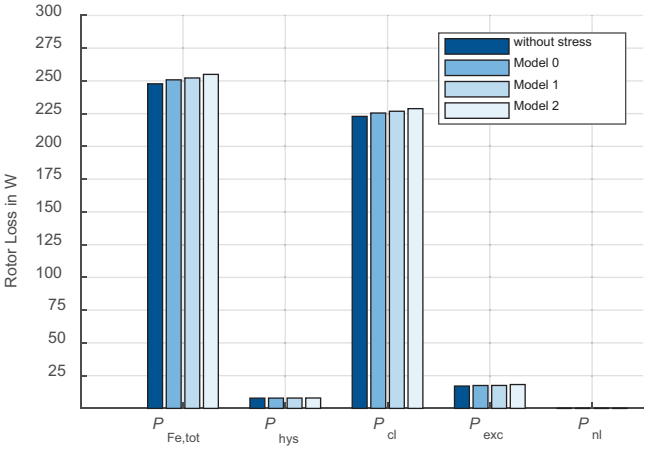

Figure 9.
Iron loss without and with consideration of magneto-elastic effect with stress-independent loss parameters

losses in the rotor without consideration of the magneto-elastic effect are $p_{Fe,tot} = 248.1$ W. In the next step, the stress-dependent change in magnetic flux density is considered for the calculation of the iron loss. For this purpose, the unmodified, stress-independent parameters for calculating the iron loss are used. The parameters are identified using the semi-physical approach presented in Steentjes *et al.* (2013). Therefore, measurements at 50 Hz of the electrical steel M400-50A were used. The results of the material characterisation can be found in Karthaus *et al.* (2018). In this characterisation, the iron losses first decrease for small mechanical tensile stress and then increases slightly. For mechanical compressive stress, a strong increase of iron losses for small stress values can be observed before reaching a saturation value. The magneto-elastic effect in use of the

different equivalent stress models shows slight deviations in the eddy current losses compared to neglecting the effect. The other loss components show a negligible deviation. According to this, the total iron loss increases. When using Model 1, the deviations are highest with p_{cl} = 2.3 per cent, but still very small. Due to the increased eddy current losses, the total iron losses in the rotor increase slightly to $P_{Fe,tot}$ = 255 W when Model 2 is used.

The next step is to study in which way the magneto-elastic effect influences the iron losses when using the stress-dependent iron loss parameters. The detailed approach is presented in Karthaus *et al.* (2018). The iron loss components are dependent on the determined equivalent mechanical stress:

$$P_{Fe,tot} = m \cdot p_{FE,tot} = m \cdot \left(p_{hys}\left(B,f,\sigma_{eq}\right) + p_{cl}(B,f) + p_{exc}\left(B,f,\sigma_{eq}\right) + p_{nl}\left(B,f,\sigma_{eq}\right)\right) \tag{11}$$

where m is the mass and p indicate the specific iron loss. The eddy current loss component p_{cl} is independent on mechanical stress (Permiakov *et al.*, 2004). The non-linear iron loss in the rotor of the reference machine is also negligible. However, there is a deviation in the hysteresis and excess losses. The hysteresis and excess losses without consideration of the magneto-elastic effect (P_{hys} = 7.94 W, P_{exc} = 17.09 W) are significantly higher than taking this effect into account. The hysteresis losses decrease when the effect is considered, because the stress-dependent iron loss parameters for positive mechanical stresses is decreasing (Karthaus *et al.*, 2018). Because the stress-dependent parameters of the hysteresis losses for negative stress values increase, the hysteresis losses for Model 1 are also increased compared to the other equivalent stress models. The hysteresis losses for Model 1 deviate by 10.6 per cent compared to the losses without consideration of the magneto-elastic effect. Similar correlations are observed for the excess losses. When using the von Mises model, the excess losses are 6.83 W and thus deviate by 60 per cent from the excess losses without consideration of the magneto-elastic effect. When using Model 2, the excess losses vary by 53.8 per cent from the excess losses without taking the effect into account. However, if Model 1 is used, the excess losses only deviate by 28.7 per cent from the excess losses without consideration of the effect (Figure 10).

Due to the high differences in the use of the equivalent stress models, the most appropriate choice of the equivalent stress model is important. Model 1 is best suited here due to the consideration of the directions of magnetic field and mechanical principal stress axis. Model 2 is only allowed for a low magnetic field (Daniel, 2013), which is not solely given in an electrical machine.

A comparison of the total iron losses with and without stress dependency is shown in Table I. Due to the high absolute values of the eddy current losses, the high differences between the iron loss proportions of hysteresis and excess losses in the total iron losses are low. The effect of the lower components in the hysteresis and excess losses are compensated by the increased eddy current losses. The total losses are reduced by a maximum amount of 3.6 per cent in relation to the iron losses without magneto-elastic effect when Model 0 is used. For Model 1, the deviation is only 0.2 per cent.

4. Conclusions

The consideration of the magneto-elastic effect leads to a significant change in the properties of the magnetic circuit, as it can be seen in the magnetic flux density or iron loss. Therefore,

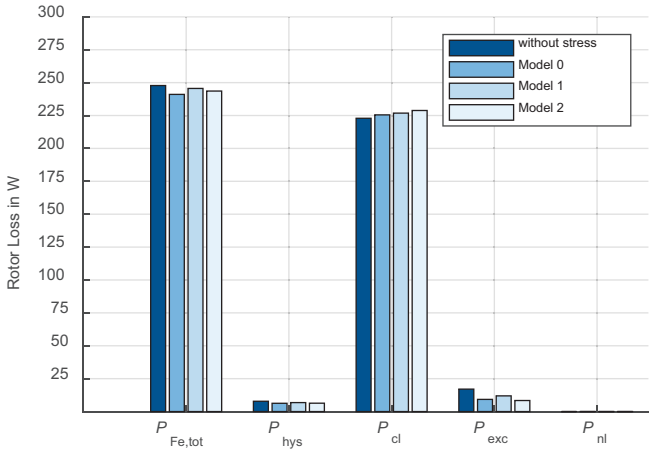

Figure 10.
Iron loss without and with consideration of magneto-elastic effect with stress-dependent loss parameters

Without consideration of magneto-elastic effect	248.1 W
With consideration of magneto-elastic effect	
Model 0	239.3 W
Model 1	247.7 W
Model 2	243.6 W

Table I.
Comparison of total rotor iron loss

considering the effect of mechanical stress on magnetic properties can be crucial for the simulation and analysis of rotating electrical machines.

In this paper, the link between mechanical stress and magnetic properties was studied with focus on the utilisation in high-speed electrical machines. Therefore, different models of equivalent mechanical stress criteria were compared and coupled with electromagnetic simulations. As results, magnetic flux density, torque and iron loss were compared.

In contrast to the other presented equivalent stress models, the direction-based equivalent stress model is the most suitable model for the usage in electrical machines. This model considers the biaxial mechanical stress (principal stress) and direction of the magnetic flux density distribution which allows an exact mapping of the real conditions in lamination stacks.

All models show a high influence on the magnetic flux density distribution when considering the magneto-elastic effect. Particular in regions with magnetic flux densities between 0.5 T and 1.5 T, the models show a difference. The influences on the magnetic air gap flux density are small. Therefore, the resulting torque does not differ much when considering the magneto-elastic effect.

The influence of mechanical stress on the rotor loss are small due to the high eddy current losses of the chosen steel grade and operating point. When using a thinner steel grade, other loss components are more dominant (Karthaus *et al.*, 2017).

In further studies, the stator of the machine will be considered, where high mechanical stress occurs inside the stator yoke due to shrink fitting of the stator stack inside the housing. Furthermore, to validate the presented models, biaxial measurements are required.

References

Aydin, U., Rasilo, P., Singh, D., Lehikoinen, A., Belahcen, A. and Arkkio, A. (2016), "Coupled magneto-mechanical analysis of iron sheets under biaxial stress", *IEEE Transactions on Magnetics*, Vol. 52 No. 3, pp. 1-4.

Aydin, U., Rasilo, P., Martin, F., Singh, D., Daniel, L., Belahcen, A., Kouhia, R. and Arkkio, A. (2017), "Modelling the effect of multiaxial stress on magnetic hysteresis of electrical steel sheets: a comparison", *IEEE Transactions on Magnetics*, Vol. 53 No. 6, p. 1.

Balluff, M., Karthaus, J., Schröder, M., Gerlach, M. and Hameyer, K. (2018), "Untersuchung der auswirkungen der statorsegmentierung auf die eigenschaften eines elektrischen kraftfahrzeugtraktionsantriebs", *e and i Elektrotechnik Und Informationstechnik*, Vol. 135 No. 2, pp. 213-222.

Daniel, L. (2013), "An analytical model for the effect of multiaxial stress on the magnetic susceptibility of ferromagnetic materials", *IEEE Transactions on Magnetics*, Vol. 49 No. 5, pp. 2037-2040.

Daniel, L. and Hubert, O. (2009), "An equivalent stress for the influence of multiaxial stress on the magnetic behavior", *Journal of Applied Physics*, Vol. 105 No. 7, p. 7.

Eggers, D., Steentjes, S. and Hameyer, K. (2012), "Advanced iron-loss estimation for nonlinear material behavior", *IEEE Transactions on Magnetics*, Vol. 48 No. 11, pp. 3021-3024.

Groschup, B. and Leonardi, F. (2017), "Combined electromagnetic and static structural simulation to reduce the weight of a permanent magnet machine rotor for HEV application", *2017 IEEE International Electric Machines and Drives Conference (IEMDC)*, 21-24 May, *Miami, FL*, 5/21/2017-5/24/2017, *IEEE, Piscataway, NJ*, pp. 1-6.

Karthaus, J. and Hameyer, K. (2017), "Static and cyclic mechanical loads inside the rotor lamination of high-speed PMSM", *2017 7th International Electric Drives Production Conference (E|DPC)*, 5th-6th December, *Wuerzburg, Germany proceedings, Würzburg*, 12/5/2017-12/6/2017, *IEEE, Piscataway, NJ*, pp. 1-6.

Karthaus, J., Elfgen, S., Leuning, N. and Hameyer, K. (2018), "Iron loss components dependent on mechanical compressive and tensile stress in non-oriented electrical steel", *International Journal of Applied Electromagnetics and Mechanics*, Vol. 59 No. 1, pp. 255-261.

Karthaus, J., Steentjes, S., Leuning, N. and Hameyer, K. (2017), "Effect of mechanical stress on different iron loss components up to high frequencies and magnetic flux densities", *COMPEL – The International Journal for Computation and Mathematics in Electrical and Electronic Engineering*, Vol. 36 No. 3, pp. 580-592.

Läpple, V. (2016), *Einführung in Die Festigkeitslehre: Lehr- Und Übungsbuch, 4., Aktualisierte Auflage*, Springer Vieweg, Wiesbaden.

Leuning, N., Steentjes, S., Schulte, M., Bleck, W. and Hameyer, K. (2016), "Effect of elastic and plastic tensile mechanical loading on the magnetic properties of NGO electrical steel", *Journal of Magnetism and Magnetic Materials*, Vol. 417, pp. 42-48.

Permiakov, V., Dupré, L., Pulnikov, A. and Melkebeek, J. (2004), "Loss separation and parameters for hysteresis modelling under compressive and tensile stresses", *Journal of Magnetism and Magnetic Materials*, Vol. 272-276, pp. E553-E554.

Sablik, M.J., Riley, L.A., Burkhardt, G.L., Kwun, H., Cannell, P.Y., Watts, K.T. and Langman, R.A. (1994), "Micromagnetic model for the influence of biaxial stress on hysteretic magnetic properties", *Journal of Applied Physics*, Vol. 75 No. 10, pp. 5673-5675.

Steentjes, S., Leßmann, M. and Hameyer, K. (2013), "Semi-physical parameter identification for an iron-loss formula allowing loss-separation", *Journal of Applied Physics*, Vol. 113 No. 17, p. 17A319-1.

Yamazaki, K. and Fukushima, W. (2015), "Loss analysis of induction motors by considering shrink fitting of stator housings", *IEEE Transactions on Magnetics*, Vol. 51 No. 3, pp. 1-4.

Yamazaki, K., Mukaiyama, H. and Daniel, L. (2018), "Effects of multi-axial mechanical stress on loss characteristics of electrical steel sheets and interior permanent magnet machines", *IEEE Transactions on Magnetics*, Vol. 54 No. 3, pp. 1-4.

Corresponding author
Jan Karthaus can be contacted at: jan.karthaus@iem.rwth-aachen.de